NACA TN 4300 10642

TECH LIBRARY KAFB, NM
0067218

NATIONAL ADVISORY COMMITTEE FOR AERONAUTICS

TECHNICAL NOTE 4300

HEAT-TRANSFER AND PRESSURE MEASUREMENTS ON FLAT-FACED CYLINDERS AT A MACH NUMBER OF 2

By William E. Stoney, Jr., and J. Thomas Markley

Langley Aeronautical Laboratory
Langley Field, Va.

Washington
July 1958

AFMDC
TECHNICAL LIBRARY

TECH LIBRARY KAFB, NM

0067218

D

NATIONAL ADVISORY COMMITTEE FOR AERONAUT

TECHNICAL NOTE 4300

HEAT-TRANSFER AND PRESSURE MEASUREMENTS ON FLAT-FACED CYLINDERS AT A MACH NUMBER OF 2

By William E. Stoney, Jr., and J. Thomas Markley

SUMMARY

Flat-faced cylinders of 12-inch diameter and 4-inch diameter were tested at a Mach number of 2 and sea-level conditions in the preflight jet of the Langley Pilotless Aircraft Research Station at Wallops Island, Va. Both pressure distributions and heat-transfer rates were measured.

The pressure data from the 4-inch-diameter model agreed well with the results of several other investigations. The stagnation-point pressure gradient was indicated to be about 30 percent of the gradient on an equivalent-size hemisphere. The heat-transfer data agreed reasonably well with the theoretical results when the flow was laminar. The stagnation-point heating rates were approximately 55 percent as great as the stagnation heating rates on a hemisphere of equal diameter.

INTRODUCTION

On a reentry ballistic missile, the area most seriously affected by aerodynamic heating usually is the nose. A pointed nose may be desirable because of its low drag characteristics but is undesirable because the heat-transfer coefficient is extremely large at the tip in relation to the mass available to absorb the incoming heat. One method of alleviating this heating problem is to blunt the nose. The blunting reduces the heat-absorption problem by two means. First, the heat-transfer coefficient is an inverse function of the square root of the nose radius of curvature and thus is reduced by blunting, and second, much greater amounts of material are available for heat absorption.

The flat-faced cylinder is the simplest of all blunt-nose shapes. Theoretically the flat nose has the lowest stagnation-point heating rates (with the possible exception of concave shapes). For these reasons a series of tests on flat-faced cylinders was made to obtain the heat-transfer and pressure distributions on this shape, and the results are presented in this report. Four models were tested, two 12-inch-diameter models and two 4-inch-diameter models. All tests were conducted with

the face of the cylinder normal to the airstream for a Mach number of 2 in a free jet at Wallops Island, Va. True sea-level conditions existed during all tests.

SYMBOLS

a	speed of sound, ft/sec
c_w	specific heat of skin, Btu/(lb)(°R)
D	diameter of hemisphere
h	aerodynamic heat-transfer coefficient, Btu/(sec)(sq ft)(°R)
$h_s = \frac{h_l}{h_{o,hemi}}$	
k	thermal conductivity, Btu/(sec)(sq ft)(°R/ft)
l	distance from corner of cylinder to shock (measured at an angle of 67° with center line), in.
M	Mach number
N_{Nu}	Nusselt number
N_{Pr}	Prandtl number
N_{St}	Stanton number
p	static pressure, lb/sq ft
Q	total heat input
q	heating rate, Btu/(sec)(sq ft)
R	Reynolds number per foot
R_θ	Reynolds number based on momentum thickness
r	radius of model, in.
T	temperature, °R
t	time, sec

U	velocity, ft/sec
$\frac{dU}{dx}$	velocity gradient
x	distance along front surface from center line of model, in.
γ	ratio of specific heats of air
δ	distance from center of face of cylinder to shock, in.
μ	coefficient of viscosity, slugs/ft-sec
η_r	recovery factor
ρ	density of atmosphere, slugs/cu ft
ρ_w	density of skin, lb/cu ft
τ_w	wall thickness, in.

Subscripts:

aw	adiabatic wall
hemi	hemisphere
l	local value at edge of boundary layer
$l$am	laminar
o	stagnation point
r	based on maximum radius
turb	turbulent
w	wall
∞	free stream ahead of shock

APPARATUS AND TESTING

Test Facility

All tests were conducted at the preflight jet of the Langley Pilotless Aircraft Research Station at Wallops Island, Va. This blowdown jet, which

is discussed more fully in reference 1, has a Mach number of 2 and sea-level conditions. The models were located with their center line on the axis of the jet and their face 2 inches downstream of the nozzle. The 4-inch heat-transfer model in the 12- by 12-inch jet is shown in figure 1 and the 4-inch pressure model in the 27- by 27-inch jet is shown in figure 2.

Models

The characteristics and number of runs for each of the four models are presented in table I. The locations of the thermocouples and pressure orifices are shown in figure 3, and the construction details, representative of models A and B and closely similar to those of model C, are shown in figure 4. All models were backed by mahogany disks cut out around the thermocouple locations as shown in figure 4.

Range of Tests

All models were tested normal to the airstream at a Mach number of 2. Model A, model B, and model D were tested in the 27- by 27-inch free jet, and model C was tested in the 12- by 12-inch free jet and the 8-inch-diameter free jet. For models A, B, and D, pressure and temperature conditions did not vary as much as 1 percent from those shown in figure 5. For model C, similar conditions prevailed. The heating rates of this report are from data obtained at the earliest time at which the jet conditions reached the steady state. The times marked in figure 5 are representative of all the tests. The total temperature and total pressure remained constant for about 8 seconds after the steady state was reached. At the time for which the heating rates were calculated the temperatures at the edge had already risen about 100° above those at the center, as shown by the typical temperature histories in figure 6.

Data Reduction

The heat-transfer coefficients were calculated after steady flow conditions were established in the jet. The following equation was used:

$$h = \frac{\rho_w c_w \tau_w}{T_{aw} - T_w} \frac{dT_w}{dt}$$

The time rate of change of wall temperature was obtained from plots of the wall temperature as a function of time. The heat-transfer coefficient was then evaluated by using a density for Inconel of 518 lb/cu ft and its

specific heat as given in reference 2. The measured values of skin thickness were used in all calculations.

The adiabatic wall temperature was obtained from

$$T_{aw} = T_o\left[\eta_r\left(1 - \frac{T_l}{T_o}\right) + \frac{T_l}{T_o}\right]$$

with η_r assumed to be equal to $N_{Pr}^{1/2}$. Actually, whether the laminar or the turbulent recovery factor η_r is used makes little difference since the minimum ratio of T_l/T_o on the body was 0.84.

The equation used to calculate the heating rates assumes constant temperature through the wall thickness, negligible heat flow laterally in the plate, negligible heat flow due to radiation, and negligible heat loss to the backing material. It is easy to show that all these conditions were true for these tests with the exception of the heat flow to the backing material. At times up to 2 seconds the jet had not come up to full operating pressure. The variation in the heating rates up to this time was due largely to the varying pressure in the jet and thus these data were not usable. Analyses of the data gathered at later times than those used in the data reduction indicated rapidly decreasing values of heat-transfer coefficient with time. These reductions are far greater than theory indicates the increasing wall temperature with time could cause. It is believed that these apparently decreasing rates are due to heat losses to the backing material, even though there is only air directly behind the thermocouple locations, and it is assumed that for all the data presented this loss is less than 20 percent at the early times for which the data are presented. The losses at the extreme edge station may be larger, since the edge was cantilevered from the backing material and was thus exposed to the low-pressure air and possible turbulence of the external flow. It must be noted, however, that to date it has not been possible to calculate heat losses of the magnitude required to keep the heat transfer constant. A more detailed discussion of this subject is presented in appendix A.

RESULTS AND DISCUSSION

Pressure Measurements

Pressure distributions.- The pressures measured on model D (4-inch-diameter model) are presented in figure 7 as fractions of the total pressure behind the shock, and are compared with available theoretical and

experimental distributions. Pressures were also measured on the 12-inch-diameter model A; however, the pressures were measured more accurately on model D and these results are felt to be most reliable. It also appears that the measurements on the 12-inch model were sufficiently different from those on the 4-inch model to indicate the possibility of some interaction between the 12-inch model and the jet. A detailed discussion of these measurements on the 12-inch model is presented in appendix B.

The open and solid points represent measurements on the two sides of the main ray and their agreement is a measure of the symmetry of the flow field over the face. A dashed line has been drawn through the solid symbols for the 4-inch model to indicate what is believed to be a reliable pressure distribution at $M = 2$. The pressures indicated by the solid symbols were measured by low-range cells which measured the difference between the local pressure and the pressure at the center tube, and thus are considerably more reliable at most of the stations than the remaining measurements, which were made with total-pressure instruments of higher range.

Test results at a Mach number of 2.01 on a 3-inch-diameter flat face have been presented in reference 3. The points obtained from figure 4 of this reference compare well with the data of the present report. (See fig. 7.) Tests of a 4-inch-diameter model have recently been made in the Langley Unitary Plan wind tunnel at $M = 2.49$. These results also compare well with the present data.

The solid lines in figure 7 represent the theoretical results of Maccoll and Codd (ref. 4) which were calculated for $M = 1.50$ by a rather tedious iterative method. These results had to be taken from a fairly rough plot, and thus some of the difference shown may be due to inaccurate transcription instead of the difference in Mach numbers.

Velocity distributions.- All the pressure measurements shown in figure 7 have been substituted into the compressible Bernoulli equation

$$\frac{U_l}{a_o} = \sqrt{\frac{2}{\gamma - 1}\left[1 - \left(\frac{p_l}{p_o}\right)^{\frac{\gamma-1}{\gamma}}\right]}$$

where a_o, the stagnation speed of sound, is

$$a_o = \sqrt{\gamma \frac{p_o}{\rho_o}}$$

in order to obtain the values of U_l/a_o presented in figure 7. The value of U_l/a_o is used simply because it is a function that depends on the

pressure ratio alone. This parameter is sensitive to small changes in pressure ratio near $\frac{p_l}{p_o} = 1$. The velocity ratios of the various tests compare well, even near the stagnation point where accurate measurements are very difficult because of the small pressure gradients existing there.

The comparison of the measurements at Mach numbers of 2 and 2.49 indicates that the effect of Mach number on pressure ratio and velocity ratio is small over this range. The difference between these values and the theoretical calculations for $M = 1.50$ may be real but the possibility of an inadequacy in the theory (or the transcription of its results) must be kept in mind.

Velocity gradient.- The heat transfer at the stagnation point is proportional to the square root of the velocity gradient at the stagnation point. As can be seen from the pressure ratios in figure 7, the local pressures are very little different from the stagnation-point pressures, and thus extremely sensitive pressure measurements must be made near the stagnation point if the velocity gradient is to be presented accurately in figure 8. The velocities from the present test and from the test in the Unitary Plan wind tunnel have been replotted to a larger scale in figure 8 and compared with values taken from reference 3. Though these points from reference 3 are from the same test as the points shown in figure 7, the points in figure 8 were obtained from figure 13 of reference 3, which presents a function of the velocity ratio rather than simply pressure ratio, and thus some small differences may be noticed between the values presented in figures 7 and 8. In addition to the increased sensitivity of the velocity-ratio function, data from all four rays along the body of reference 3 are presented in figure 8. The top line has been faired through the two points from present tests and the lower line has been faired through the data from reference 3. The scatter in the data from reference 3 is large and the points available from the present tests are few; thus no significant difference is shown. Fortunately there is also only a small difference between the velocity gradients indicated, since the present data give $\frac{r}{a_o}\frac{dU}{dx} = 0.33$ and those of reference 3 give $\frac{r}{a_o}\frac{dU}{dx} = 0.31$.

It should be pointed out that the authors of reference 3 did not analyze their data in the same manner, and they obtained a value of $\frac{r}{a_o}\frac{dU}{dx} = 0.36$. This difference is caused by the apparently low velocity-ratio values which were measured at their first station, since they faired a straight line through the data from each ray and averaged the resultant slopes. This method seems to place too much weight on the measurements at the first station, which the scatter alone indicates are the least accurate,

since it does not allow the fairing to include the 0 value of the stagnation point. This effect can also be noted in figure 18 of reference 3, where the fairing may be taken to indicate a value of $\frac{r}{a_o}\frac{dU}{dx} = 0.305$.

Local properties.- The remaining local values of importance are shown in figure 9. The local densities and temperatures obtained from the line faired through the data for the 4-inch model are divided by their stagnation-point values, while the local Reynolds numbers and the product of density and velocity are presented as fractions of the free-stream value.

Since there is some indication that the local pressure ratio p_l/p_o remains invariant with Mach number or at least increases only slightly with increasing Mach number, these local values may be used to approximate conditions on a flat nose at higher Mach numbers. The only local values that change directly with Mach number are the product of density and velocity and the local Reynolds number ratio. Thus, under this assumption, for an ideal gas the local density-velocity product at $M = 10$ and 15 would be 20 percent larger than at a Mach number of 2, while the ratio of local to free-stream Reynolds number would be only 0.48 of the $M = 2$ value at $M = 10$, and 0.34 of the $M = 2$ value at $M = 15$.

Heat-Transfer Measurements

Stagnation-point heat transfer.- Stagnation-point heating rates are presented in figure 10 for both the 4-inch-diameter and 12-inch-diameter models. The values for the 4-inch models were measured at the stagnation point, whereas those for the 12-inch models were obtained by averaging the rates measured at $\frac{x}{r} = 0.25$. It is assumed that the theoretical results for the distribution of local heating rates (see discussion in following section) are essentially correct in their prediction of a small difference (≤ 8 percent) in rates at $\frac{x}{r} = 0.25$ and $\frac{x}{r} = 0$. There are two uncertainties involved in making this assumption for the 12-inch models: (1) the flow is probably turbulent over the outer part of the model and could possibly be so at $\frac{x}{r} = 0.25$ and (2) the measurements of local flow conditions did vary slightly from the measurements on the 4-inch model in the same jet. However doubtful the assumption may be, its use does lead to reasonable results, as can be seen by the comparison of measured and calculated values shown in figure 10.

The theory used for the calculation is that developed by Sibulkin for the flow at the stagnation point of a hemisphere (ref. 5). The same result is arrived at in references 6 and 7. This equation

$$N_{Nu,D} = 0.763 N_{Pr}^{0.4} D\left[\frac{\rho\left(\frac{dU}{dx}\right)_o}{\mu}\right]^{1/2}$$

may be written (for $N_{Pr} = 0.72$ and air properties based on wall temperature):

$$h\sqrt{r} = 0.67 k_w \sqrt{R_\infty}\sqrt{\frac{T_o}{T_w}\frac{\rho_o}{\rho_\infty}\frac{\mu_\infty}{\mu_l}\frac{1}{M_\infty}\left(\frac{T_o}{T_\infty}\right)^{1/2}}\sqrt{\frac{r}{a_o}\left(\frac{dU}{dx}\right)_o} \tag{1}$$

where R_∞ is the free-stream Reynolds number per foot. With the proper values of $\left(\frac{dU}{dx}\right)_o$ this equation is applicable to any shape. The value measured in the present test, $\frac{R}{a_o}\left(\frac{dU}{dx}\right)_o = 0.32$, was used in the calculations of figure 10. The stagnation-point heat-transfer coefficient from the test of the 4-inch model in the Unitary Plan wind tunnel at $M = 2.49$ is also shown, together with the corresponding theoretical curve computed from equation (1). The difference in level is due to the fact that the Reynolds number per foot was 2.7×10^6 in the Unitary Plan wind tunnel and 14×10^6 for the other data in figure 10. Again the theory and experiment are in good agreement (the measured value of h is 0.009 and the theoretical value is 0.0083).

Local heat-transfer distributions.- The ratio of local heat-transfer coefficients to the measured values at the stagnation point are presented in figure 11. Heat-transfer measurements were also made in the Unitary Plan wind tunnel during the test for which pressure data has been presented in figure 7. The values from all four rays on the Unitary tunnel model are also presented in figure 11, the spread being indicated by the extensions on the symbols (the large spread at the edge is actually due to only one low point). The data from the 12-inch models include results from four runs along many rays, and again the spread of the data is indicated by the vertical extensions.

These measured values are compared with theoretical laminar distributions calculated by the method of Lees (ref. 6) and the method of Stine and Wanlass (ref. 8), and also with a turbulent distribution derived from flat-plate theory. The details of all these calculations are discussed in appendix C.

It is apparent that all the data except those for the 12-inch model are clustered about the two laminar distributions, and it seems reasonable

to assume that all the bodies except the 12-inch model have entirely laminar flow on their surfaces. Though the scatter is large, the data appear to agree with the Lees distribution better than with the Stine and Wanlass distribution, in spite of the violation of Lees' assumption that $\frac{T_w}{T_o} \ll 1$. The Stine and Wanlass method, which is simply the two-dimensional boundary-layer solution corrected by the Mangler transformation and applied for the given local pressure gradient, appears to be too sensitive to the high pressure gradients found near the edge of the face. This sensitivity may be the reason why it seems to be in greater error for the flat face than for the hemisphere, where it has previously been shown to be quite accurate; the gradients on the hemisphere are considerably lower than those near the edge of the flat face.

The greater spread in the data near the edge of the 12-inch model is due in part to the greater rate of change with time exhibited by the heat-transfer rates at these points (see appendix A). The downward trend noticeable in the Unitary Plan tunnel data is probably due to lateral heat flow around the corner, since that model, unlike the models of the present investigation, had a continuous metal connection with its cylindrical section.

The heat-transfer distribution measured on the 12-inch model is strikingly different from that on the 4-inch model, and the obvious reason for the difference would be the presence of turbulent flow on the 12-inch model and not on the 4-inch model. As mentioned previously and as discussed more fully in appendix B, the pressures measured on the 12-inch model were somewhat different from those measured on the 4-inch model; however, neither of the laminar theories exhibits a pressure sensitivity large enough to account for the large change in heat-transfer rates measured. It would appear that this difference in local conditions is not the cause of the difference in heat-transfer coefficients, and this belief is somewhat borne out by the comparison with the modified flat-plate turbulent rates shown in figure 11. The turbulent equation derived in appendix C is similar to that derived in reference 9. In the reference report the comparison between the theoretical flat-plate values and the measured values was fairly good, but the nose was hemispherical, and as mentioned before the higher gradients of the flat face stretch the assumptions of the flat-plate theory more severely than the generally lower hemispherical values. The data obtained on the sides of a cone with a hemispherical tip (ref. 10) also can be shown to agree with the modified flat-plate theory, and here again the low pressure gradients may account for the better agreement.

Local Reynolds number distributions.- If the data for the 12-inch model do represent transitional or turbulent heat-transfer rates, it is interesting to compare the local Reynolds number distribution on the two bodies. Figure 12 presents both the local Reynolds number and the

local Reynolds number based on momentum thickness (see appendix C for calculation method) for each size body. In either case, if it is assumed that the data for the four-inch model indicate entirely laminar flow, the difference in local Reynolds numbers would not predict that the flow on the 12-inch model would turn turbulent as near the center as it apparently did $\left(\frac{x}{r} \approx 0.4 \text{ or } 0.5\right)$. Thus some doubt remains as to the cause of transition on the 12-inch model. It was noted that the 12-inch model was more severely pitted by particles from the jet than the 4-inch model.

Comparison of hemisphere and flat-face heating rates.- A comparison between the heating rates on a flat face and on a hemisphere can easily be made if all the local rates are divided by the stagnation-point heating rate for a hemisphere of the same size. Such a comparison is presented in figure 13. The laminar calculations of Lees (ref. 6) for both the hemisphere and the flat face are shown, as well as the apparently turbulent values for the 12-inch flat face and for the hemisphere tested at the same Reynolds number and Mach number. The maximum turbulent heat transfers are about the same, and it would seem that the location of transition would have to be known to enable a rational choice between the two shapes on the basis of low maximum local heating rates. However, if the flow is completely laminar, the maximum local value for the flat face is 15 percent less than that for the hemisphere.

Another comparison may be made on the basis of total heat input. In this case it is important to remember that the hemisphere has twice as much skin area as the flat face. A comparison of total turbulent rates from these tests is not very valuable since the ratio of turbulent to laminar heating rate is a function of local Mach number, and thus results of one test are not directly applicable to another. An integration of the laminar curves of figure 13 shows that, at $M = 2$,

$$\frac{Q_{flat}}{Q_{hemi}} = 0.7$$

SUMMARY OF RESULTS

From tests made in the preflight jet at a Mach number of 2 and sea-level Reynolds number on flat-faced models of two different sizes (12-inch and 4-inch diameter) the following results were obtained:

1. The pressures measured on the face of the 4-inch model agreed very well with the results of two other tests. These pressure measurements allow the determination of a reliable value of the velocity gradient at the stagnation point; that is,

$$\frac{r}{a_o}\left(\frac{dU}{dx}\right)_o = 0.32$$

where r is the maximum radius, a_o is the speed of sound at the stagnation temperature, and $\left(\frac{dU}{dx}\right)_o$ is the velocity gradient. This is about 30 percent of the gradient on a hemisphere of equal diameter. Comparison with measurements at a Mach number of 2.5 indicates that this value may not change significantly for Mach numbers above 2.

2. When this stagnation-point velocity gradient was used, the measured stagnation-point heat-transfer rates agreed well with the theoretical predictions. The measured rates were approximately 55 percent of those which would be measured on a hemisphere of equal diameter.

3. The distribution of the heating rates over the surface indicated that the flow was entirely laminar on the 4-inch model and was turbulent over most of the 12-inch model. The laminar data compared reasonably well with the theories used, but a turbulent theory derived from flat-plate theory gave heat-transfer rates higher than the measured rates on the 12-inch face.

Langley Aeronautical Laboratory,
National Advisory Committee for Aeronautics,
Langley Field, Va., May 2, 1958.

APPENDIX A

VARIATION OF MEASURED QUANTITIES WITH TIME

The purpose of this appendix is to discuss in some detail a phenomenon treated somewhat superficially in the body of the report, namely, the apparent variation with time of the heat-transfer coefficients. As mentioned in the body of the report, it is the opinion of the authors that the data as presented represent fairly well the true heat-transfer coefficients and that their variation with time is only an apparent one due to the loss of an unknown amount of heat to the backing material.

Temperature-time histories for the stations at $\frac{x}{r} = 0.25$ and $\frac{x}{r} = 0.97$ are presented in figure 14. These are representative of data having the maximum and minimum variations of heating rate with time. The time history of the apparent heating rates $\left(q = \rho_w c_w \tau_w \frac{dT_w}{dt}\right)$ obtained from these temperature histories is presented in figure 15. Up to 2 seconds, the flow in the jet has not reached design pressures as is shown by the total-pressure and total-temperature records presented in figure 5, and the q variations up to this time can be assumed to be due to this starting flow. If the h values assumed in the report are correct, after 2 seconds the two dashed lines in figure 15 represent the heating rates which should have been measured. The temperature which would have been measured in these cases is shown by the solid lines in figure 14. The difference between the dashed and solid lines then is the apparent heat loss to the backing material.

There is little question that losses of such magnitude are possible if the material behind the plate is wood and the contact is fairly good. However, there were sizable holes $\left(1\frac{1}{4}\right.$ inches in diameter and 1 inch deep$\left.\right)$ behind most of the thermocouple locations, and it is the mechanism of the heat loss in this situation that is in question. This heat flow seems too large to be attributed to free convection, although, admittedly, this opinion is derived from analyses of infinite vertical plates which may not be applicable to this case. To add a bit more confusion to the question, the data furnished by several thermocouples which were very closely surrounded by the wood backing (see fig. 4) were essentially indistinguishable from the data furnished by the thermocouples with the large holes behind them.

As mentioned in the report, the data for the edge thermocouples may be in error on the low side because of the greater apparent heat loss shown in figure 15. The holes behind the edge thermocouples were open to the free stream and thus a greater heat loss might be expected.

APPENDIX B

PRESSURES MEASURED ON 12-INCH MODEL

The pressures measured on the 12-inch-diameter model A are presented in figure 16(a) and compared with the faired results from the 4-inch-diameter model. The difference is apparently outside the range of accuracy indicated by the spread of the data points. Figure 16(b) shows the pressures measured at the 75-percent stations at several azimuthal positions. Again the small scatter indicates that a real asymmetry may exist. This asymmetry and the pressure differences between the 12-inch model and the 4-inch model may be an indication of some type of interaction between the 12-inch model and the 27-inch jet. If such an interaction is present at all, it apparently is not a large one since the local flow conditions are not changed extensively. The operating pressure ratio of the 27-inch jet was nearly identical for the 12-inch and 4-inch models, and this fact implies little or no interference. Further indication of the smallness of the interaction, if any, is obtained from the shadowgraphs taken during the runs.

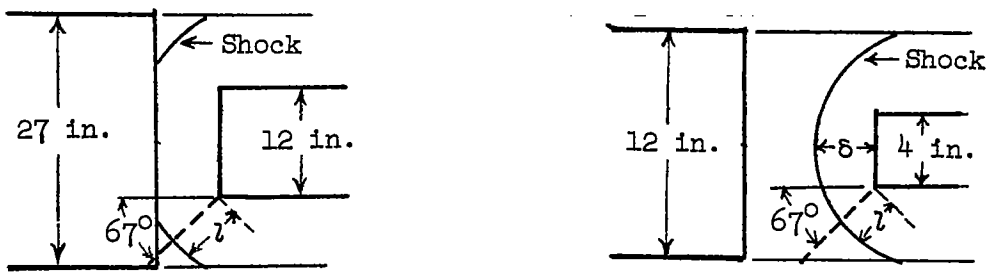

(a) 27-inch jet. $l/r = 0.868$.

(b) 12-inch jet with model backed away from nozzle. $l/r = 0.864$.

Sketch (a) represents a shadowgraph of a 12-inch model during one of the test runs, while sketch (b) shows a shadowgraph of a special run of the 4-inch model C for which it was backed away from the mouth of the jet to allow the full nose shock to be seen. Measurements of the distance from the corner of the body to the shock, measured at an angle of 67° with the center line, gave the ratios of l/r noted on the sketches. Since these ratios are essentially identical, it indicates that the shocks formed in both cases are similar. In sketch (b) the distance of the shock away from the surface can be measured and is found to be 0.752r, which is

close to the separation distance shown in reference 11 for a Mach number of 2 $\left(\frac{\rho_\infty}{\rho_o} = 0.166\right)$. Therefore, no interference was present in this test. Likewise it can be inferred that there was little or no interaction in the 12-inch tests.

In connection with this comparison, it should be noted that the ratio of model area to jet area was 0.155 for the 12-inch model in the 27-inch jet and 0.087 for the 4-inch model in the 12-inch jet. The 4-inch model was also tested in the 8-inch jet (an area ratio of 0.25), and the heat-transfer rates from both runs agreed well.

APPENDIX C

THEORETICAL HEAT-TRANSFER DISTRIBUTIONS

Laminar Distributions

Lees (ref. 6) gives the following relation:

$$\frac{q_l}{q_o} = \frac{\frac{1}{2}\frac{\rho_l}{\rho_o}\frac{U_l}{a_o}\frac{\mu_l}{\mu_o}\frac{x}{r}}{\sqrt{\int \frac{\rho_l}{\rho_o}\frac{U_l}{a_o}\frac{\mu_l}{\mu_o}\left(\frac{x}{r}\right)^2\frac{dx}{r}}}\;\frac{1}{\sqrt{\frac{r}{a_o}\left(\frac{dU}{dx}\right)_o}} \tag{2}$$

Note that Lees' expression was derived on the assumption that $\frac{T_w}{T_l} \ll 1$, which is not true in the present case. This ratio is equal to the heat-transfer coefficient ratio if $T_{aw} - T_w$ is considered constant over the surface.

The method of Stine and Wanlass (ref. 8) yields the following expression:

$$\frac{h}{h_o} = \frac{\left(\frac{N_{Nu}}{\sqrt{R}}\right)_l}{\left(\frac{N_{Nu}}{\sqrt{R}}\right)_o}\sqrt{\frac{\frac{\rho_l}{\rho_o}\frac{\mu_o}{\mu_l}\frac{U_l}{a_o}\left(\frac{k_l}{k_o}\right)^2}{\frac{r}{a_o}\left(\frac{dU}{dx}\right)_o\frac{x}{r}}} \tag{3}$$

where the ratio $\frac{\left(N_{Nu}/\sqrt{R}\right)_l}{\left(N_{Nu}/\sqrt{R}\right)_o}$ is a function of local Mach number and pressure gradient.

In the calculations based on these equations the local values measured on the 4-inch model were used. The Lees expression is very difficult to determine accurately at points near the stagnation point because both the numerator and the denominator approach zero fairly rapidly. The Stine and Wanlass calculation depends strongly on the local pressure gradient and this is difficult to determine accurately near the edge of the bodies of the present test.

The assumption of $\frac{T_w}{T_l} \ll 1$ allowed Lees to neglect the variation of heat-transfer coefficient with local pressure gradient. If it is assumed

that the variation with the pressure gradient is not important (though this appears to be an erroneous assumption if the solutions of Cohen and Reshotko are examined - see discussion in ref. 6) it is possible to obtain an expression for the heat-transfer ratio from the relationship

$$N_{St}\sqrt{r}\left(N_{Pr}\right)^{2/3} = \text{Constant}$$

This leads to

$$\frac{h}{h_o} = \left(\frac{N_{Pr}}{N_{Pr,o}}\right)^{1/3}\sqrt{\frac{\frac{\rho_l}{\rho_o}\,\frac{U_l}{a_o}\,\frac{\mu_o}{\mu_l}\left(\frac{k_l}{k_o}\right)^2}{\frac{r}{a_o}\left(\frac{dU}{dx}\right)_o\frac{x}{r}}} \tag{4}$$

Equation (4) is, of course, identical with the relationship derived from the Stine and Wanlass solution (eq. (3)) except for the term that depends on the local pressure gradient. (The Prandtl number ratio is approximately equal to 1.) It can be simplified somewhat if the relation $\frac{\mu_l}{\mu_o} = \left(\frac{T_l}{T_o}\right)^{\omega}$, where $\omega = 0.75$, is used. Neglecting the Prandtl number ratio gives

$$\frac{h}{h_o} = \sqrt{\frac{\frac{U_l}{a_o}\left(\frac{p_l}{p_o}\right)^{1/2}\left(\frac{k_l}{k_o}\right)^2}{\frac{x}{r}\,\frac{r}{a_o}\left(\frac{dU}{dx}\right)_o}} \tag{5}$$

The numerical values obtained from equation (5) for the present pressure distribution are close to those calculated from the Lees expression. Although this agreement may be fortuitous, it indicates that the difference between the Lees theory and the Stine-Wanlass theory shown in figure 11 is due almost entirely to the changes associated with the local pressure gradients. That the agreement is not entirely fortuitous can be seen by assuming that the local values in Lees' expression do not vary with x/r.

Turbulent Distribution

Van Driest (ref. 12) makes the assumption that local pressure gradient is not an important variable (which is certainly more true for the turbulent case than the laminar one - note the constants presented in ref. 12 for the various stagnation-point and flat-plate relationships). This assumption makes it easy to obtain the relation between local

turbulent heat transfer and local laminar heat transfer (for $N_{Pr} = 0.72$ and $T_w/T_\infty = 1$):

$$\frac{h_{l,turb}}{h_{l,lam}} = \frac{\rho_l U_l c_{w,l} N_{St,l,turb}}{\rho_l U_l c_{w,l} N_{St,l,lam}} = \frac{N_{St,l,turb}}{N_{St,l,lam}} = \frac{0.0374}{R_l^{1/5}} \frac{\frac{1}{0.93}}{R_l^{1/2}}$$

where the flat-plate constant for turbulent flow was chosen along with the stagnation-point constant for laminar flow because the results then agreed better with the present tests and with the equation and results of Beckwith and Gallagher (ref. 9). Thus,

$$\frac{h_{l,turb}}{h_{l,lam}} = 0.040R_l^{0.3}$$

If equation (5) for the ratio $\frac{h_{l,lam}}{h_o}$ is used, then the expression

$$\frac{h_{l,turb}}{h_o} = 0.040R_l^{0.3} \sqrt{\frac{\frac{U_l}{a_o}\left(\frac{p_l}{p_o}\right)^{1/2}\left(\frac{k_l}{k_o}\right)^2}{\frac{x}{r}\,\frac{r}{a_o}\left(\frac{dU}{dx}\right)_o}}$$

is obtained.

Reynolds Number Based on Momentum Thickness

The curves of R_θ shown in figure 12 were obtained by an approximate method due to Bromberg (ref. 13), where

$$R_\theta = 0.664\sqrt{\tilde{R}_l}$$

and

$$\tilde{R}_l = \frac{\rho_o a_o r}{\mu_o} \frac{\int_0^{x/r} \frac{\rho_l}{\rho_o}\frac{U_l}{a_o}\frac{\mu_l}{\mu_o}\left(\frac{x}{r}\right)^2 \frac{dx}{r}}{\left(\frac{\mu_l}{\mu_o}\right)^2\left(\frac{x}{r}\right)^2}$$

Note that Lees' expression for $\frac{h_l}{h_o}$ may be written

$$\frac{h_l}{h_o} = \frac{1}{2} \frac{\rho_l U_l}{\left[\rho_o \mu_o \left(\frac{dU}{dx}\right)_o\right]^{1/2} \tilde{R}_l^{1/2}}$$

REFERENCES

1. Faget, Maxime A., Watson, Raymond S., and Bartlett, Walter A., Jr.: Free-Jet Tests of a 6.5-Inch-Diameter Ram-Jet Engine at Mach Numbers of 1.81 and 2.00. NACA RM L50L06, 1951.

2. Lucks, C. F., Bing, G. F., Matolich, J., Deem, H. W., and Thompson, H. B.: The Experimental Measurement of Thermal Conductivities, Specific Heats, and Densities of Metallic, Transparent, and Protective Materials - Part II. AF Tech. Rep. No. 6145 (Contract No. AF 33(038)-20558), Battelle Memorial Inst., July 1952.

3. Boison, J. C., and Curtiss, H. A.: Preliminary Results of Spherical-Segment Blunt Body Pressure Surveys in the 20 Inch Supersonic Wind Tunnel at JPL. RAD Tech. Memo 2-TM-57-77 (Aerod. Sec. memo no. 152), AVCO Res. and Advanced Dev. Div., Oct. 9, 1957.

4. Maccoll, J. W., and Codd, J.: Theoretical Investigations of the Flow Around Various Bodies in the Sonic Region of Velocities. British Theoretical Res. Rep. No. 17/45, B.A.R.C. 45/19, Ministry of Supply, Armament Res. Dept., 1945.

5. Sibulkin, M.: Heat Transfer Near the Forward Stagnation Point of a Body of Revolution. Jour. Aero. Sci. (Readers' Forum), vol. 19, no. 8, Aug. 1952, pp. 570-571.

6. Lees, Lester: Laminar Heat Transfer Over Blunt-Nosed Bodies at Hypersonic Flight Speeds. Jet Propulsion, vol. 26, no. 4, Apr. 1956, pp. 259-269.

7. Reshotko, Eli, and Cohen, Clarence B.: Heat Transfer at the Forward Stagnation Point of Blunt Bodies. NACA TN 3513, 1955.

8. Stine, Howard A., and Wanlass, Kent: Theoretical and Experimental Investigation of Aerodynamic-Heating and Isothermal Heat-Transfer Parameters on a Hemispherical Nose With Laminar Boundary Layer at Supersonic Mach Numbers. NACA TN 3344, 1954.

9. Beckwith, Ivan E., and Gallagher, James J.: Heat Transfer and Recovery Temperatures on a Sphere With Laminar, Transitional, and Turbulent Boundary Layers at Mach Numbers of 2.00 and 4.15. NACA TN 4125, 1957.

10. Libby, Paul A., and Cresci, Robert J.: Evaluation of Several Hypersonic Turbulent Heat Transfer Analyses by Comparison With Experimental Data. WADC Tech. Note 57-72, ASTIA Doc. No. AD 118093, U. S. Air Force, July 1957.

11. Probstein, Ronald F.: Inviscid Flow in the Stagnation Point Region of Very Blunt-Nosed Bodies at Hypersonic Flight Speeds. WADC TN 56-395 (Contract No. AF 33(616)-2798), U. S. Air Force, Sept. 1956. (Also available from ASTIA as Doc. No. AD97273.)

12. Van Driest, E. R.: The Problem of Aerodynamic Heating. Aero. Eng. Rev., vol. 15, no. 10, Oct. 1956, pp. 26-41.

13. Bromberg, Robert: A Note on the Calculation of Momentum Thickness Reynolds Number in a Boundary Layer With Pressure Gradient. Rep. No. GM-TN-21, The Ramo-Wooldridge Corp., Guided Missile Res. Div., May 11, 1956.

TABLE I

TEST CHARACTERISTICS

Model	Diameter, in.	Material	Run	Jet size, in.	Measurements	Remarks	Model area / Jet area
A	12	0.032" Inconel	1 2 3	27 by 27 27 by 27 27 by 27	22 thermocouples and 15 pressure points	Runs 1 and 2 identical. For run 3, the disk was rotated 180° from first position.	0.155
B	12	0.064" magnesium alloy (AZ31A-0)	1	27 by 27	16 thermocouples		0.155
C	4	0.032" Inconel	1 2	8 (diam.) 12 by 12	7 thermocouples 7 thermocouples		0.25 0.087
D	4	Steel	1	27 by 27	21 pressure points		0.017

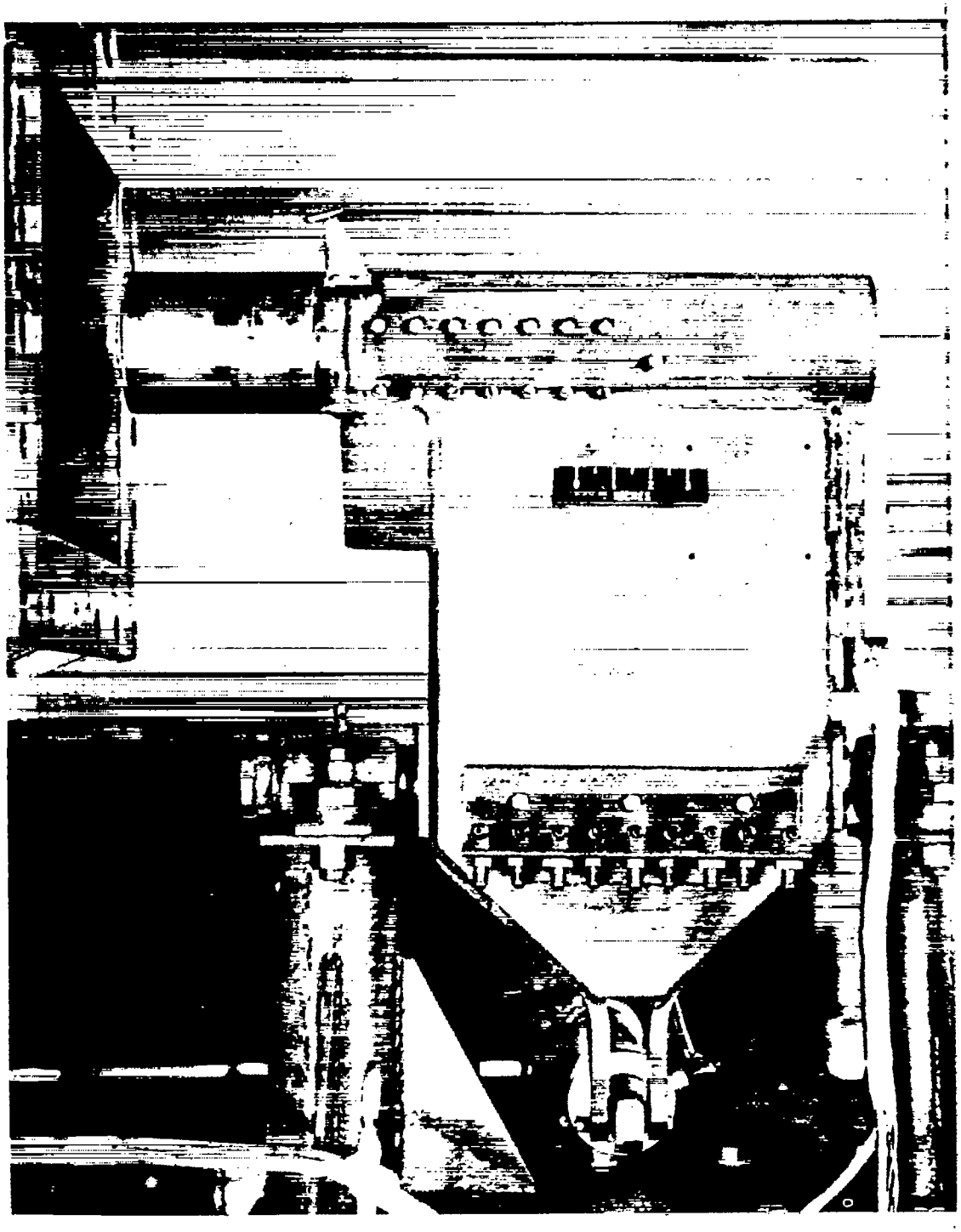

Figure 1.- Four-inch heat-transfer model in 12- by 12-inch jet. L-95238

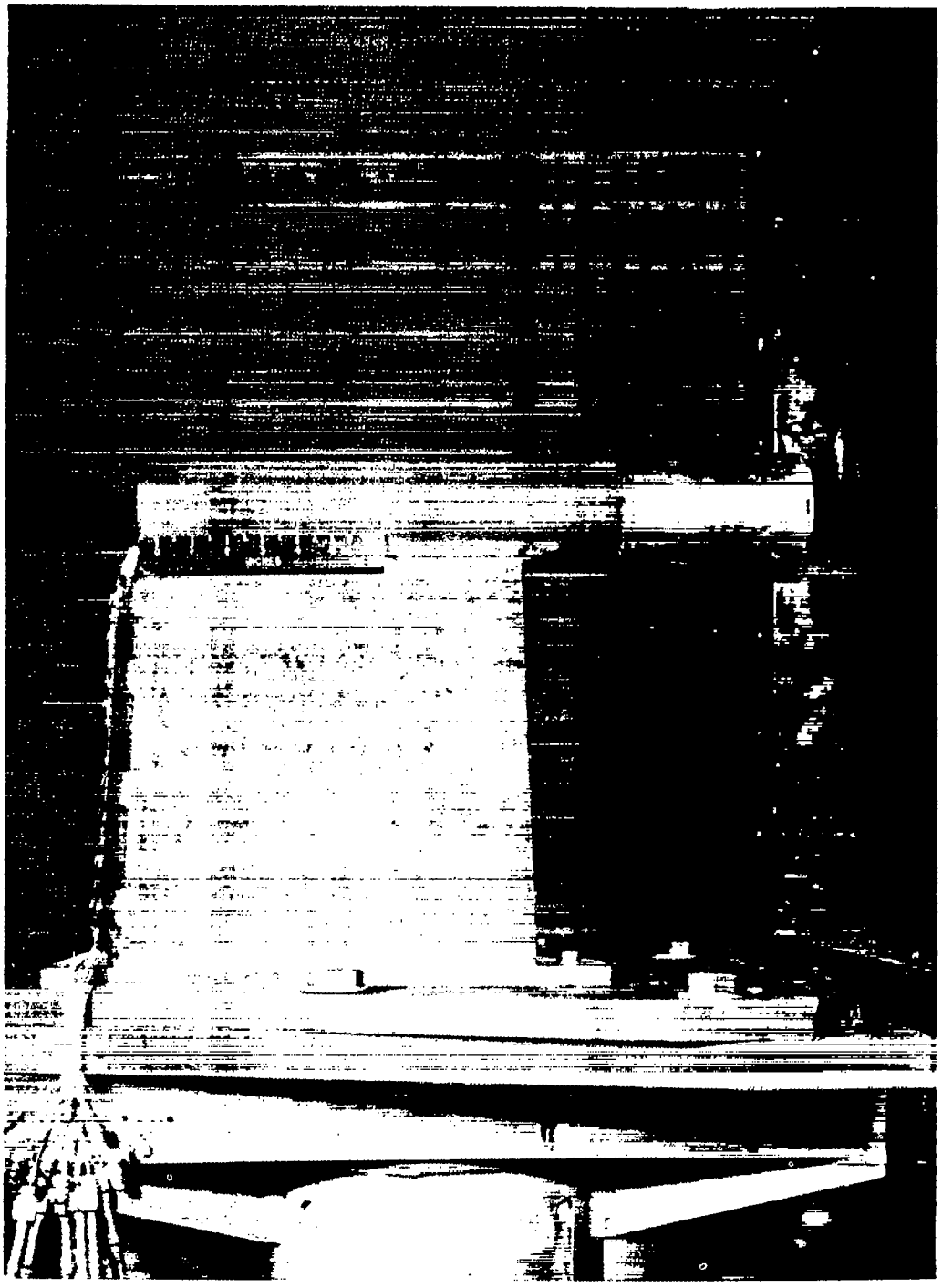

Figure 2.- Four-inch pressure model in 27- by 27-inch jet. L-57-372.1

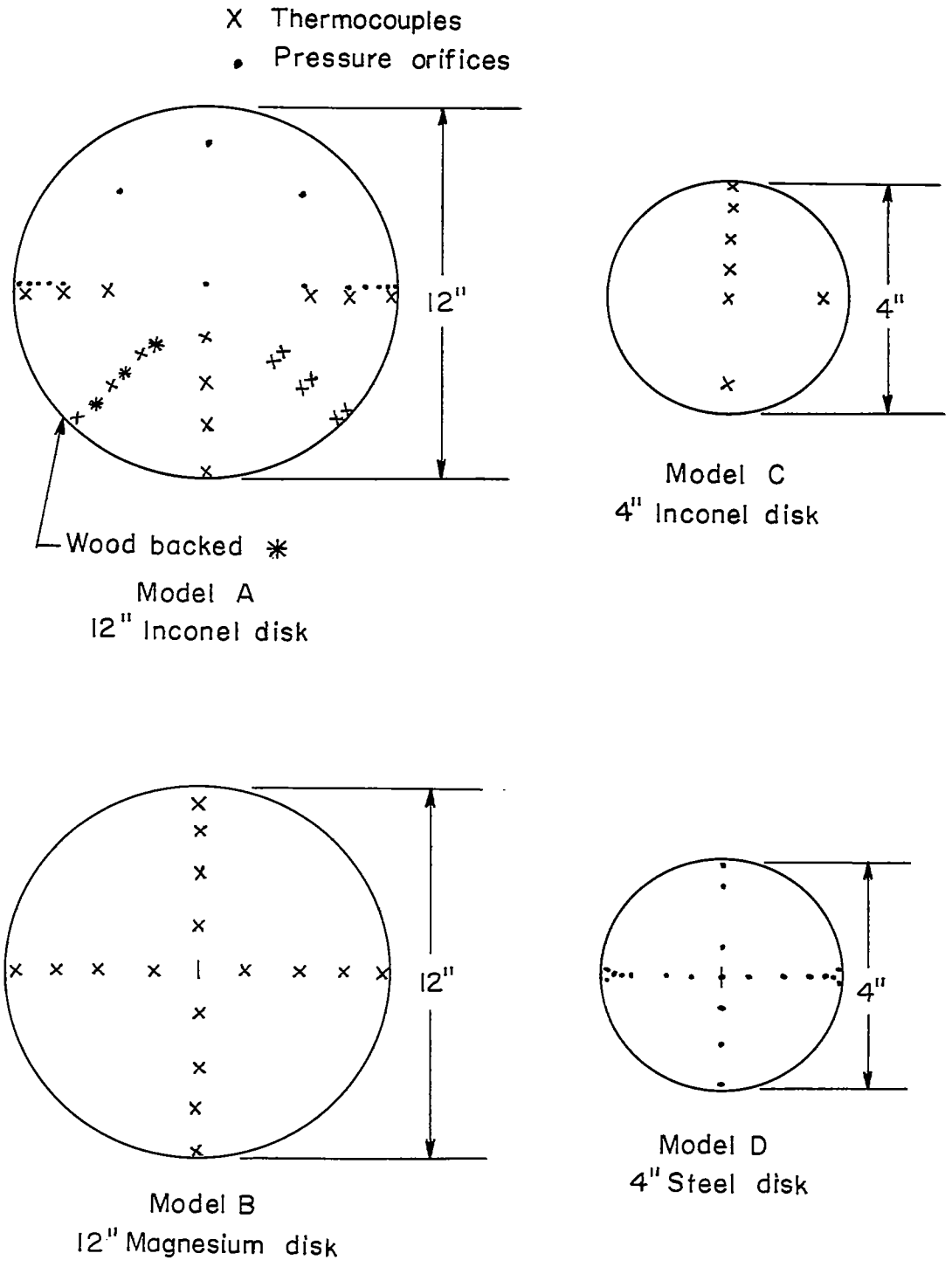

Figure 3.- Location of pressure orifices and thermocouples.

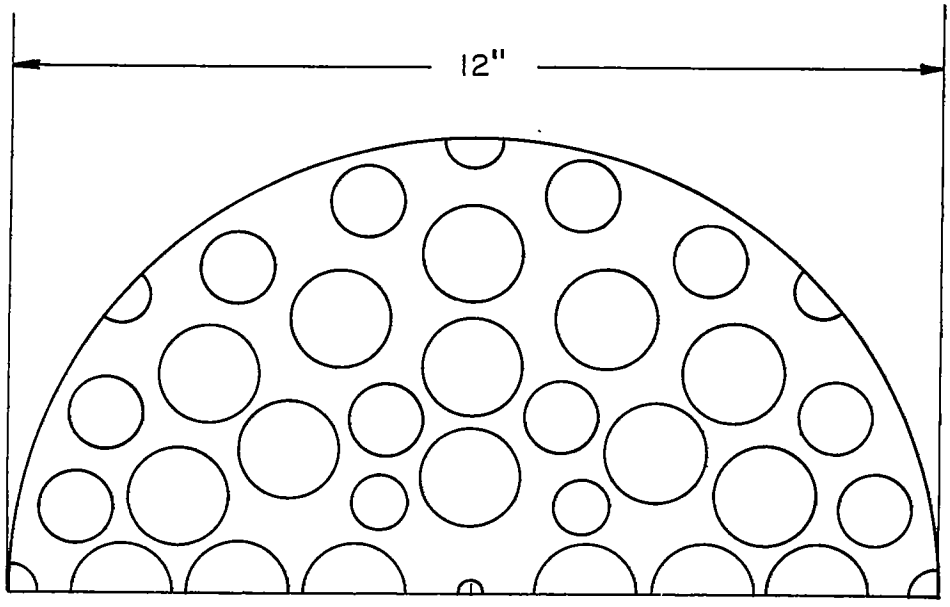

(a) Cutouts in wood backing.

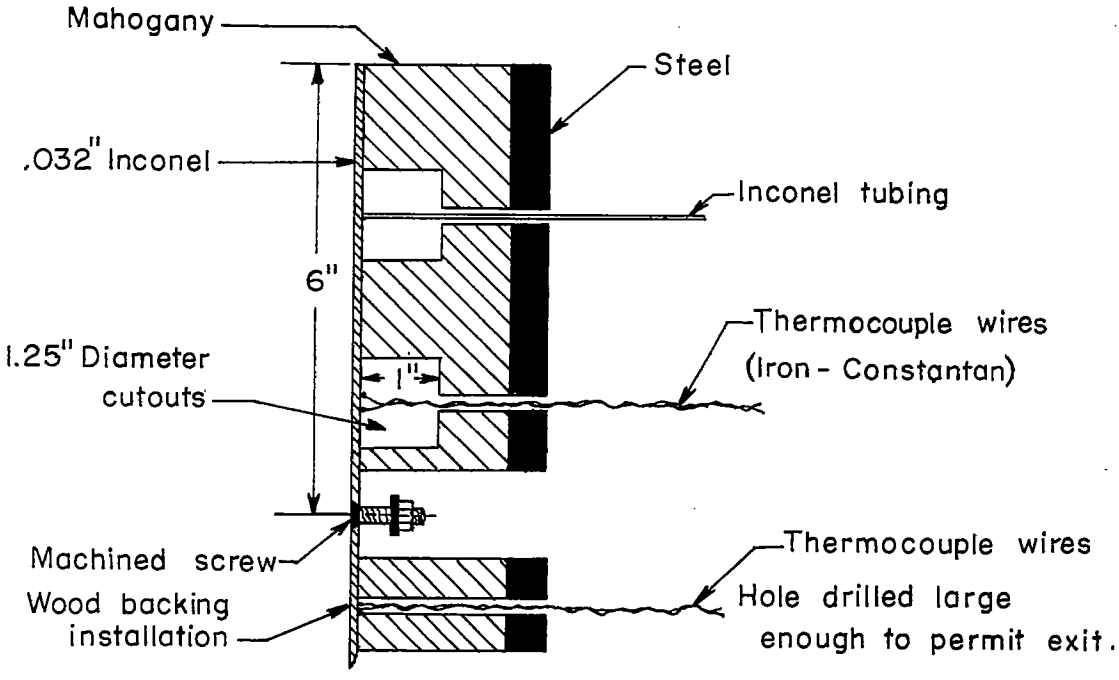

(b) Side view of model.

Figure 4.- Construction details.

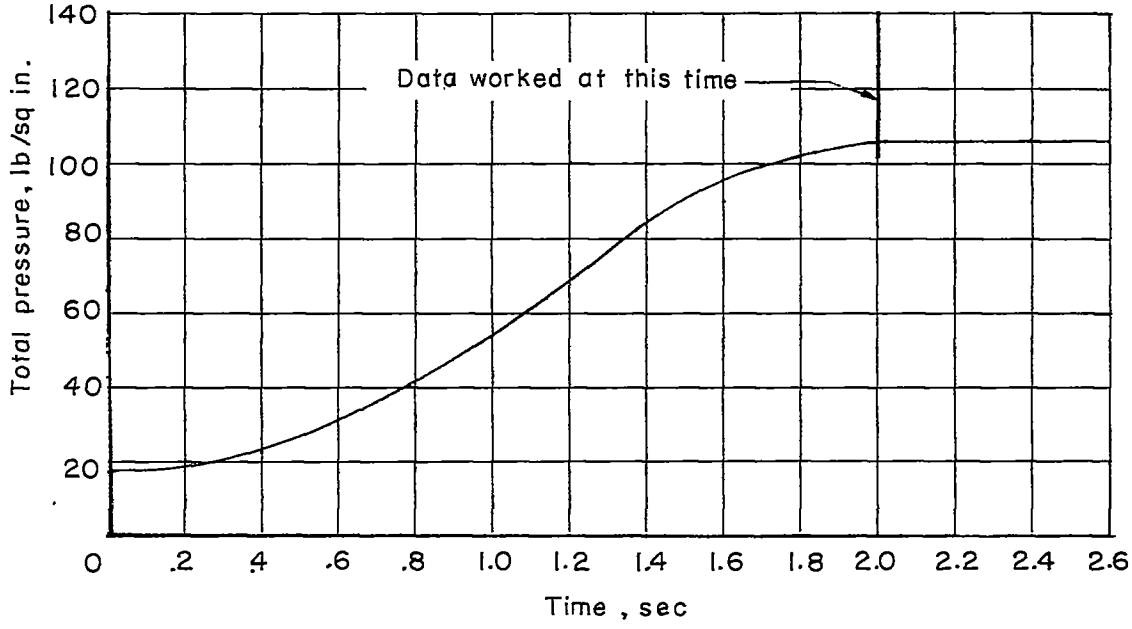

(a) Jet pressure.

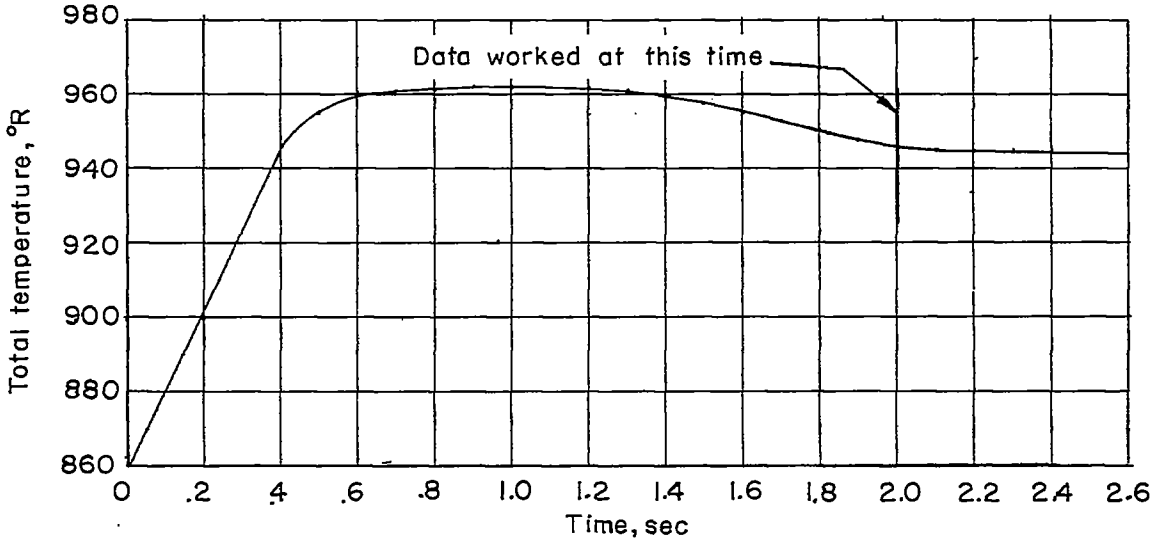

(b) Jet temperature.

Figure 5.- Jet total-temperature and total-pressure histories up to time for constant conditions.

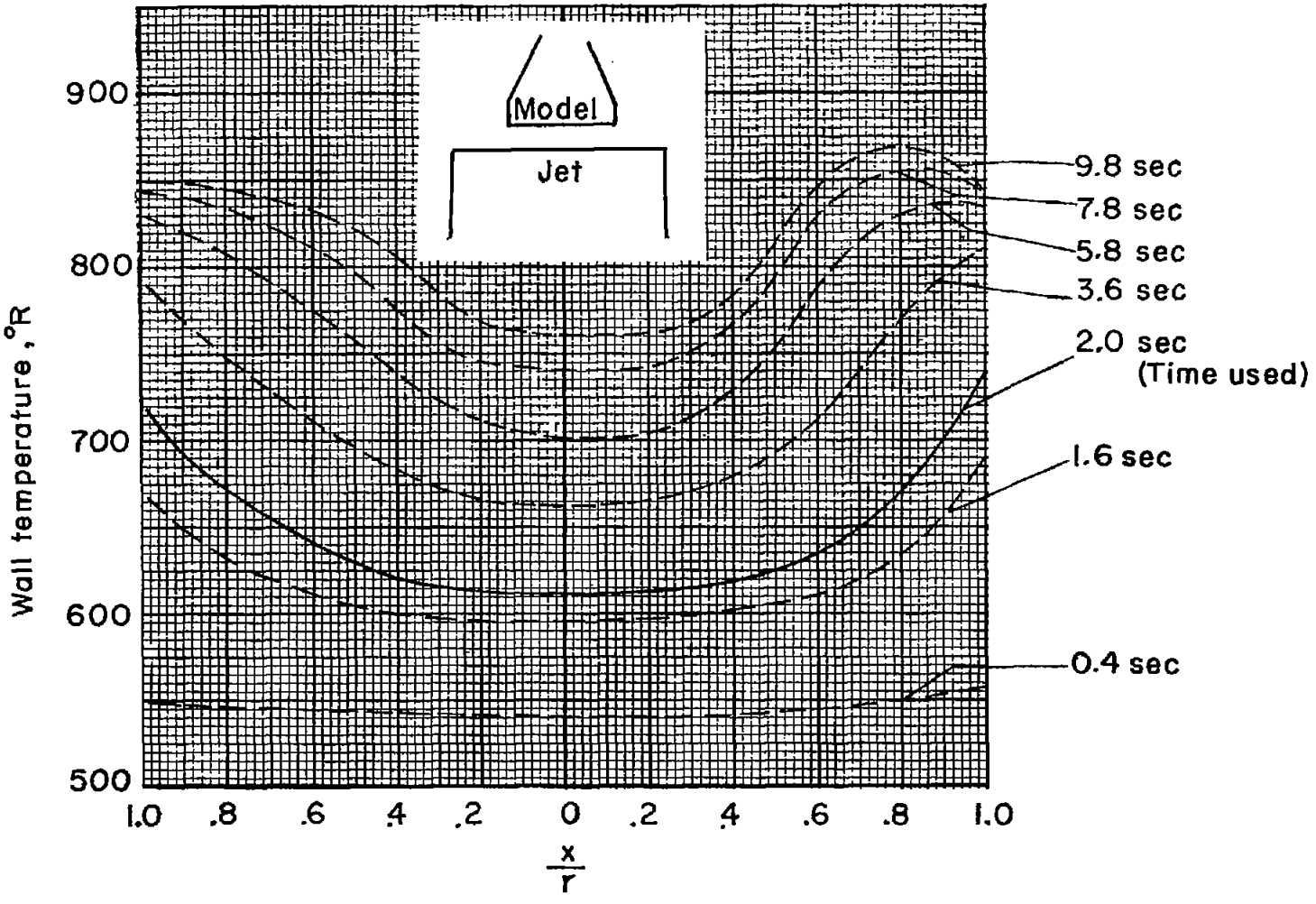

Figure 6.- Typical wall-temperature history.

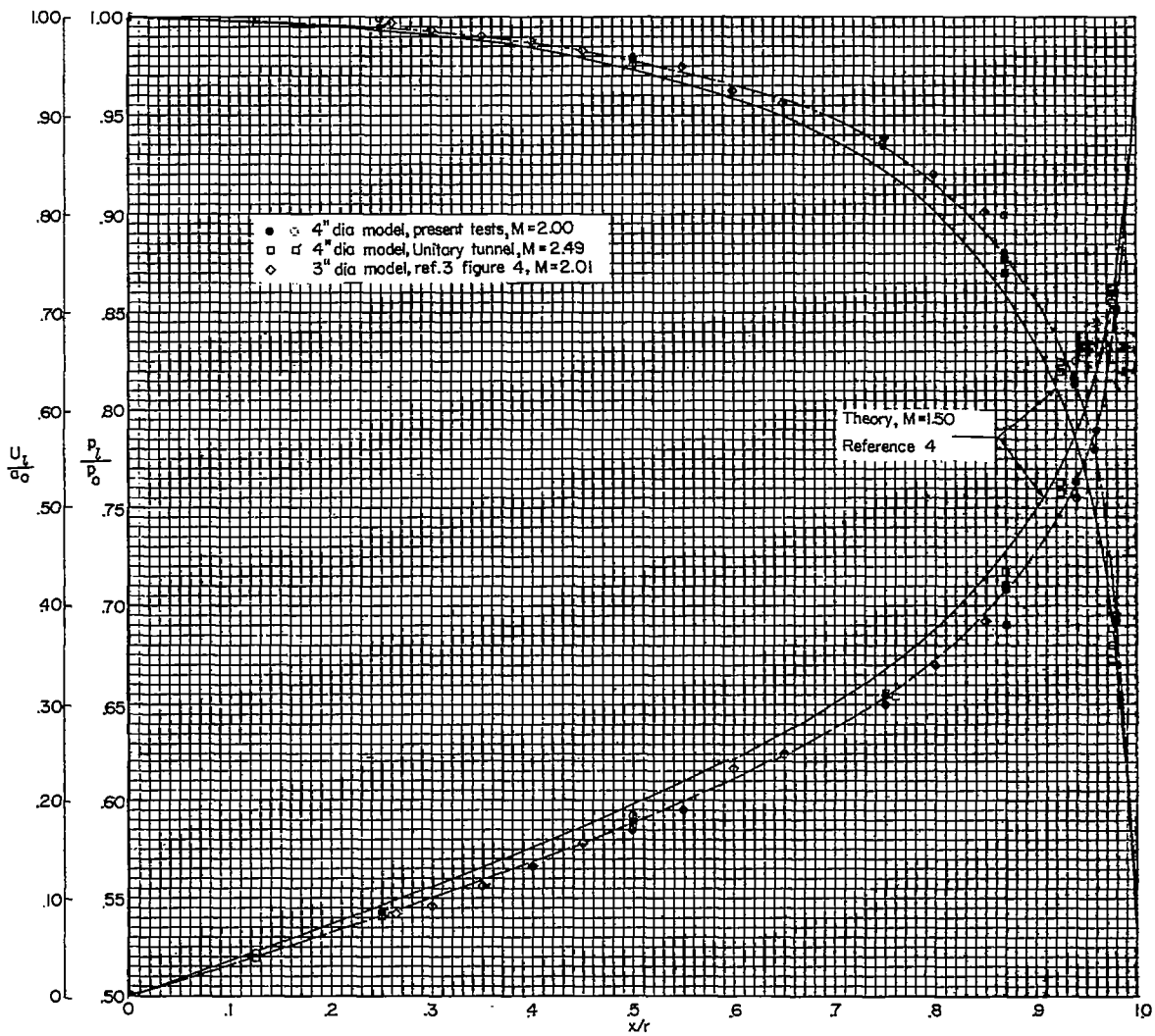

Figure 7.- Pressure distribution and velocity distribution over flat face.

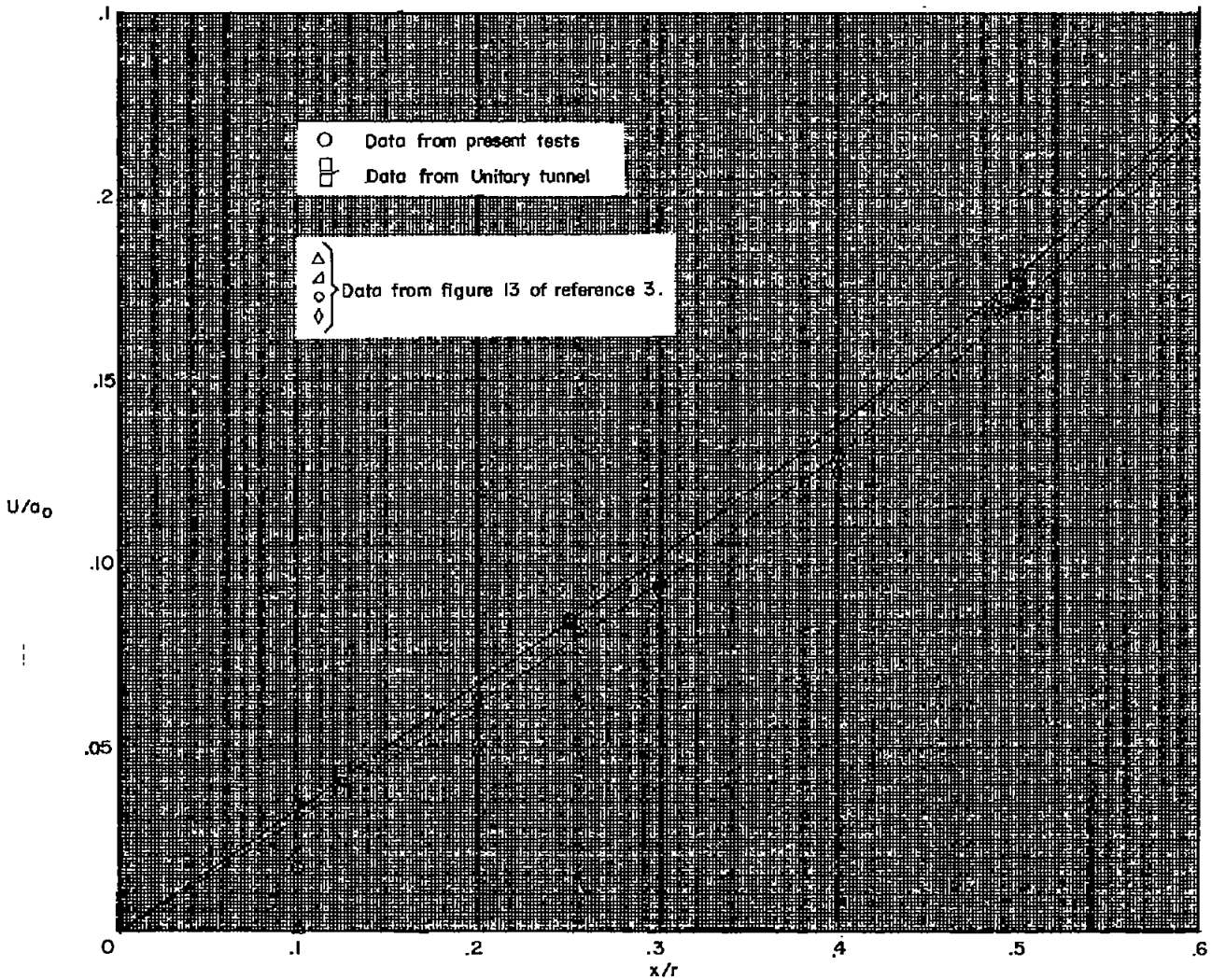

Figure 8.- Velocity ratios near the stagnation point.

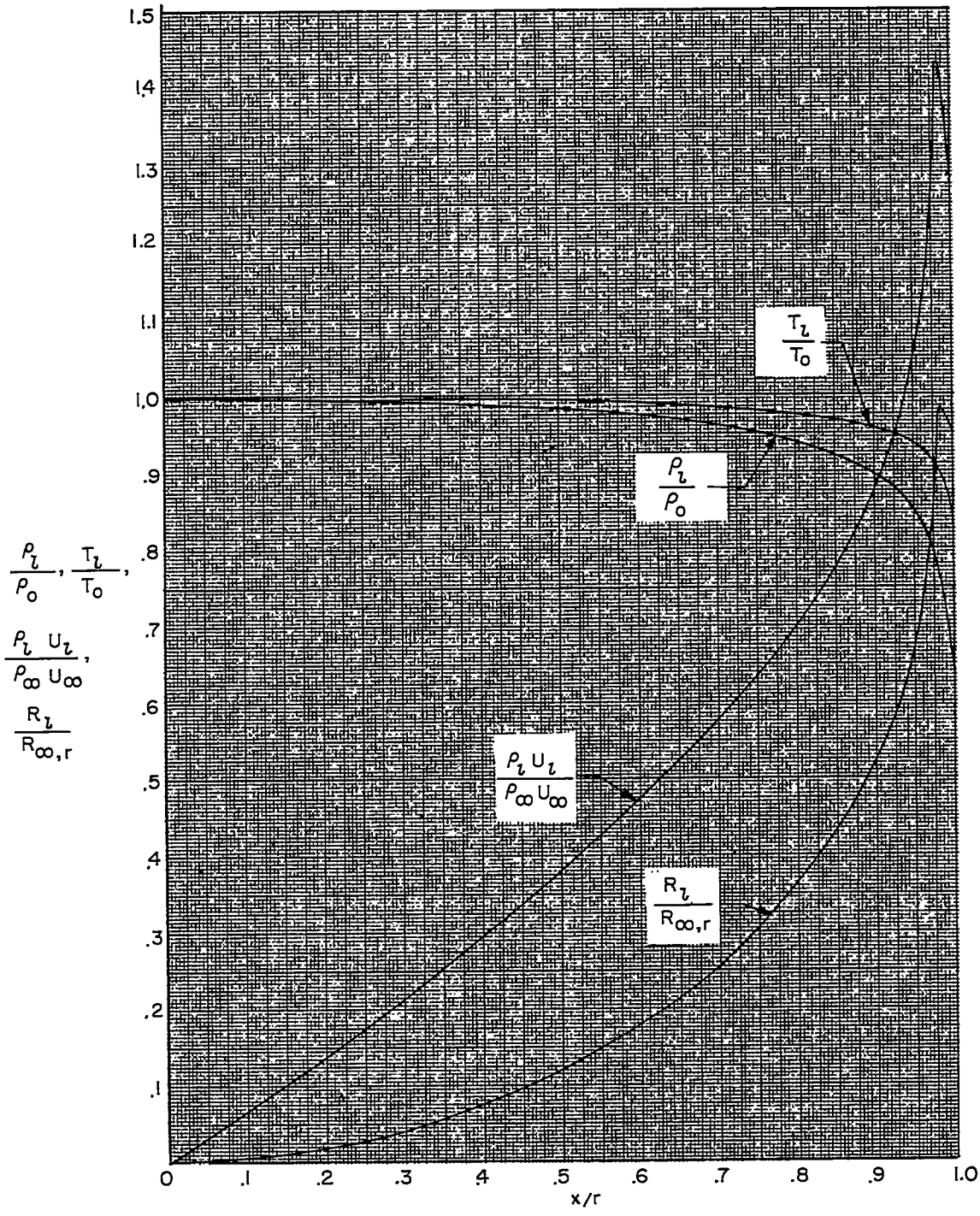

Figure 9.- Local flow properties at M = 2.

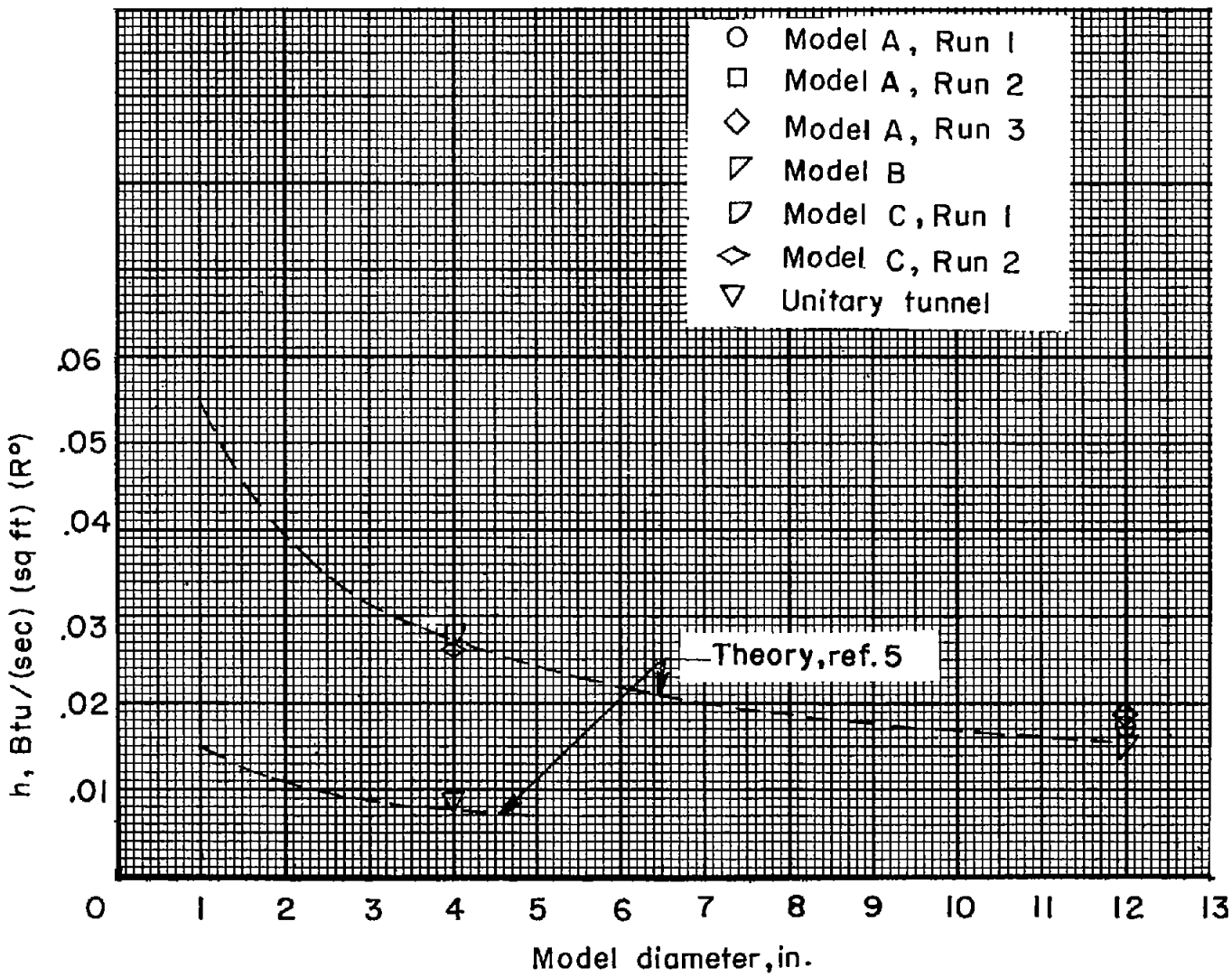

Figure 10.- Stagnation-point heat transfer on flat face.

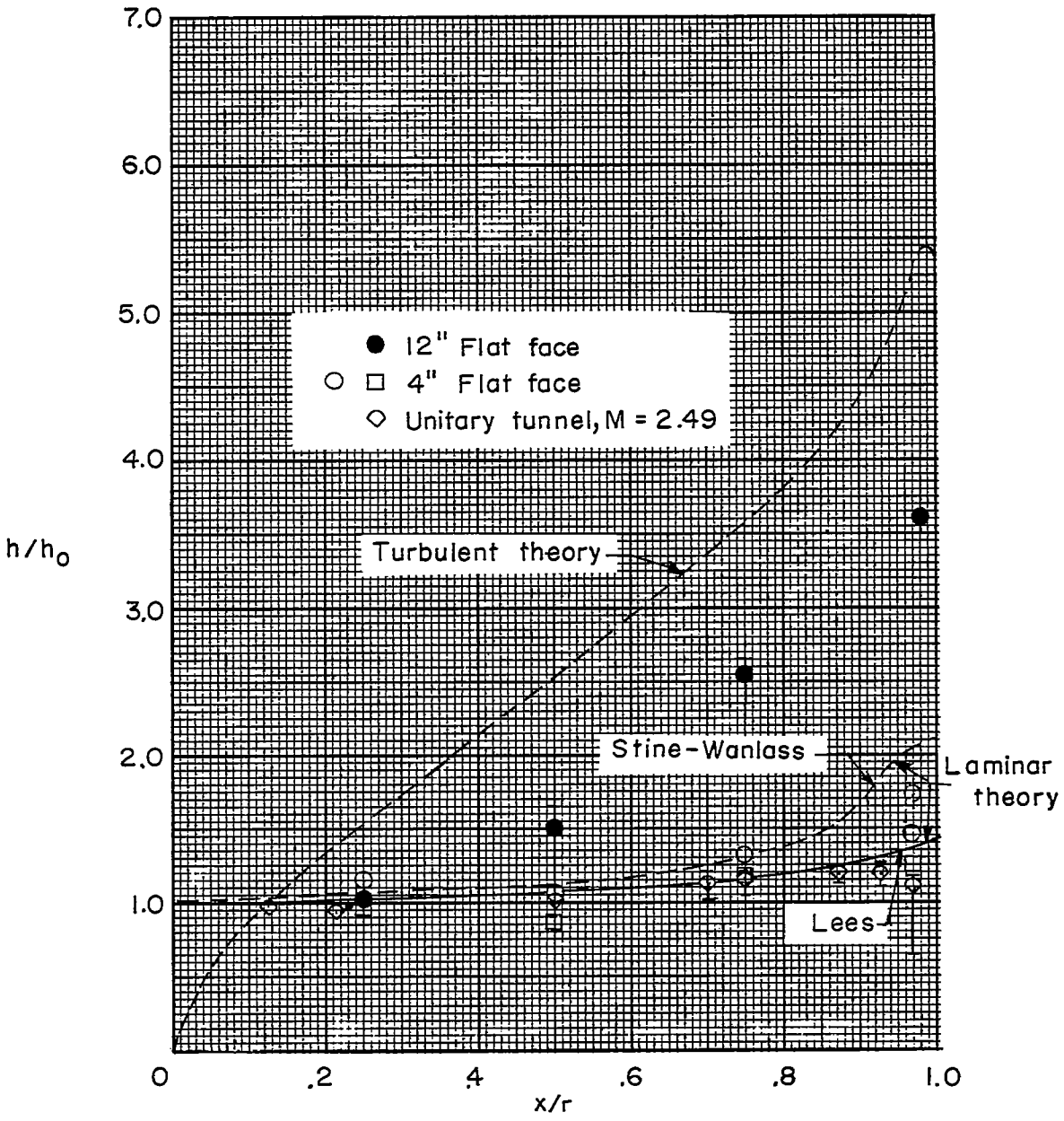

Figure 11.- Heat transfer on flat face at Mach number of 2.

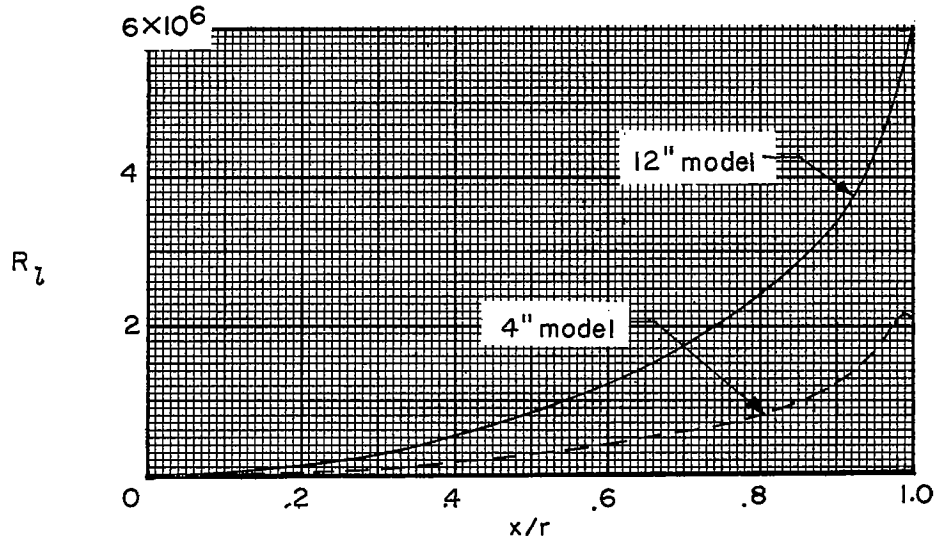

(a) Local Reynolds numbers.

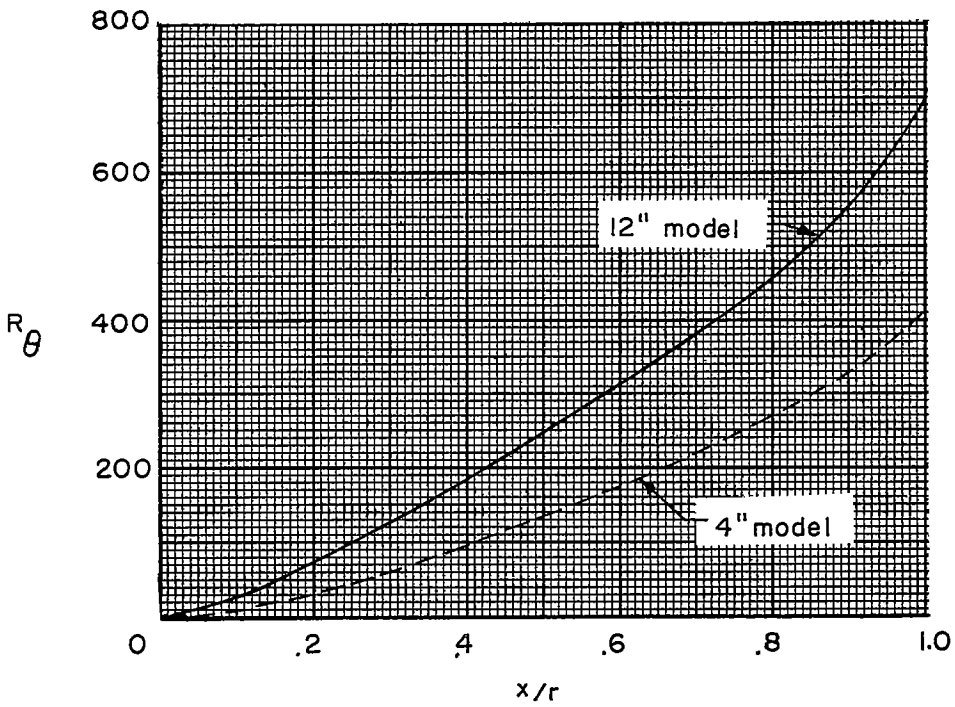

(b) Momentum-thickness Reynolds numbers.

Figure 12.- Local and momentum-thickness Reynolds numbers.

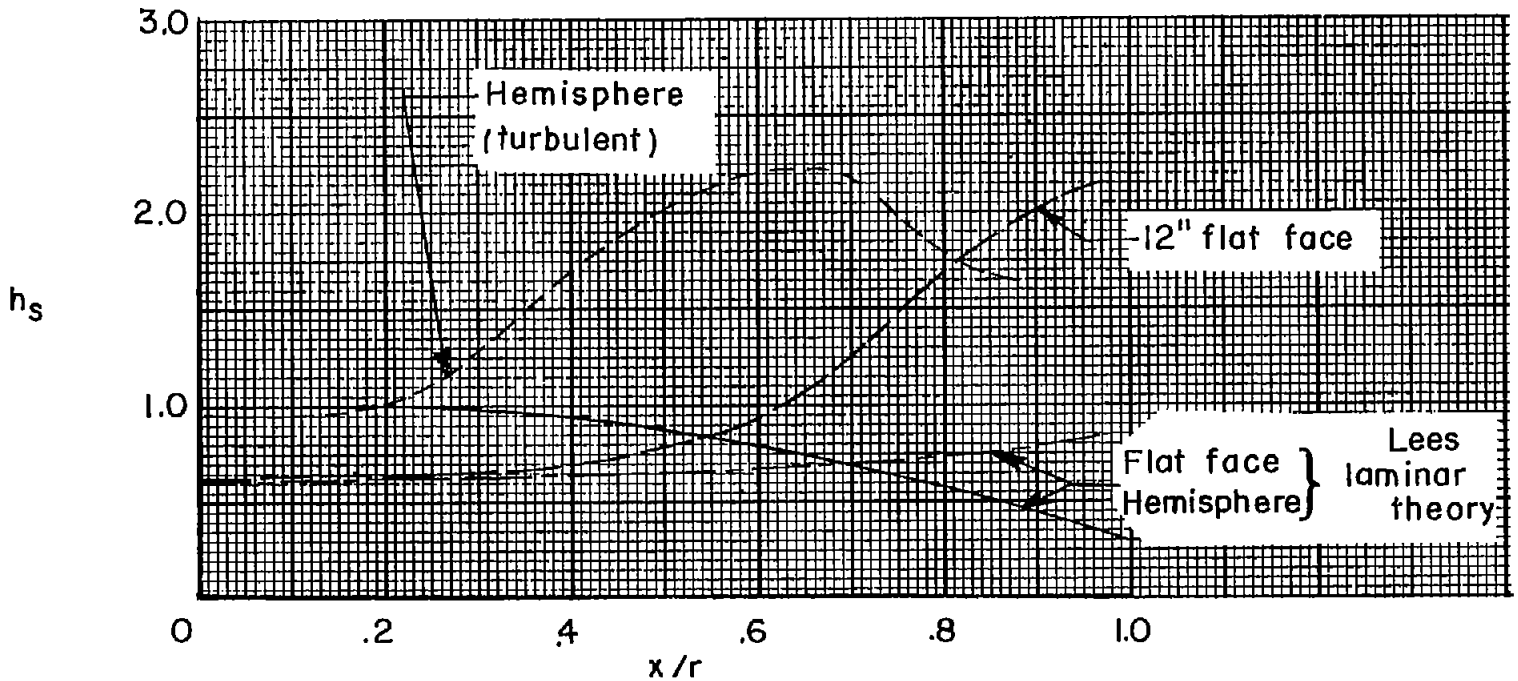

Figure 13.- Comparison of local heating rates on a flat face with those on a hemispherical surface. $h_s = \frac{h_l}{h_{o,hemi}}$.

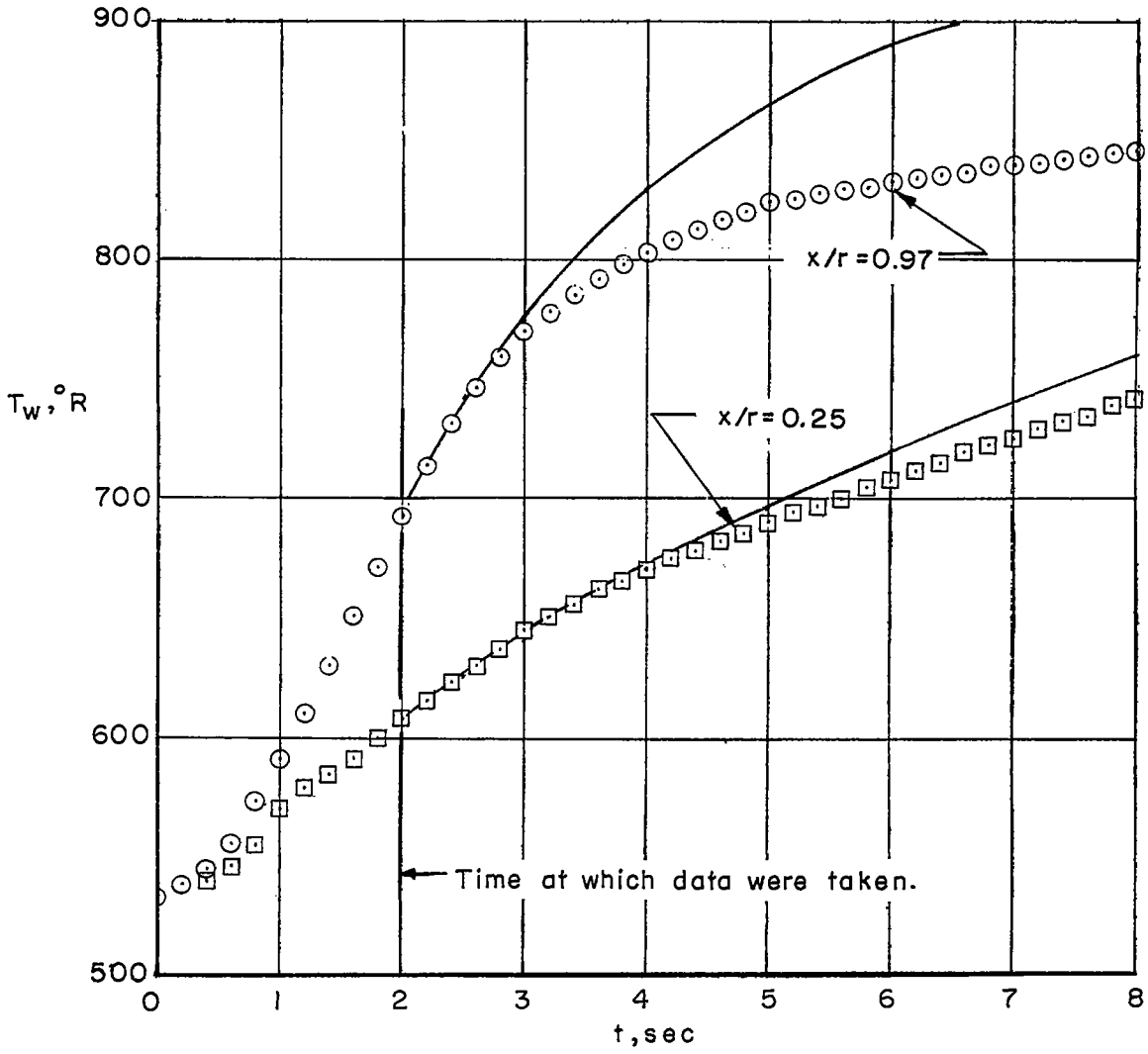

Figure 14.- Typical temperature-time histories.

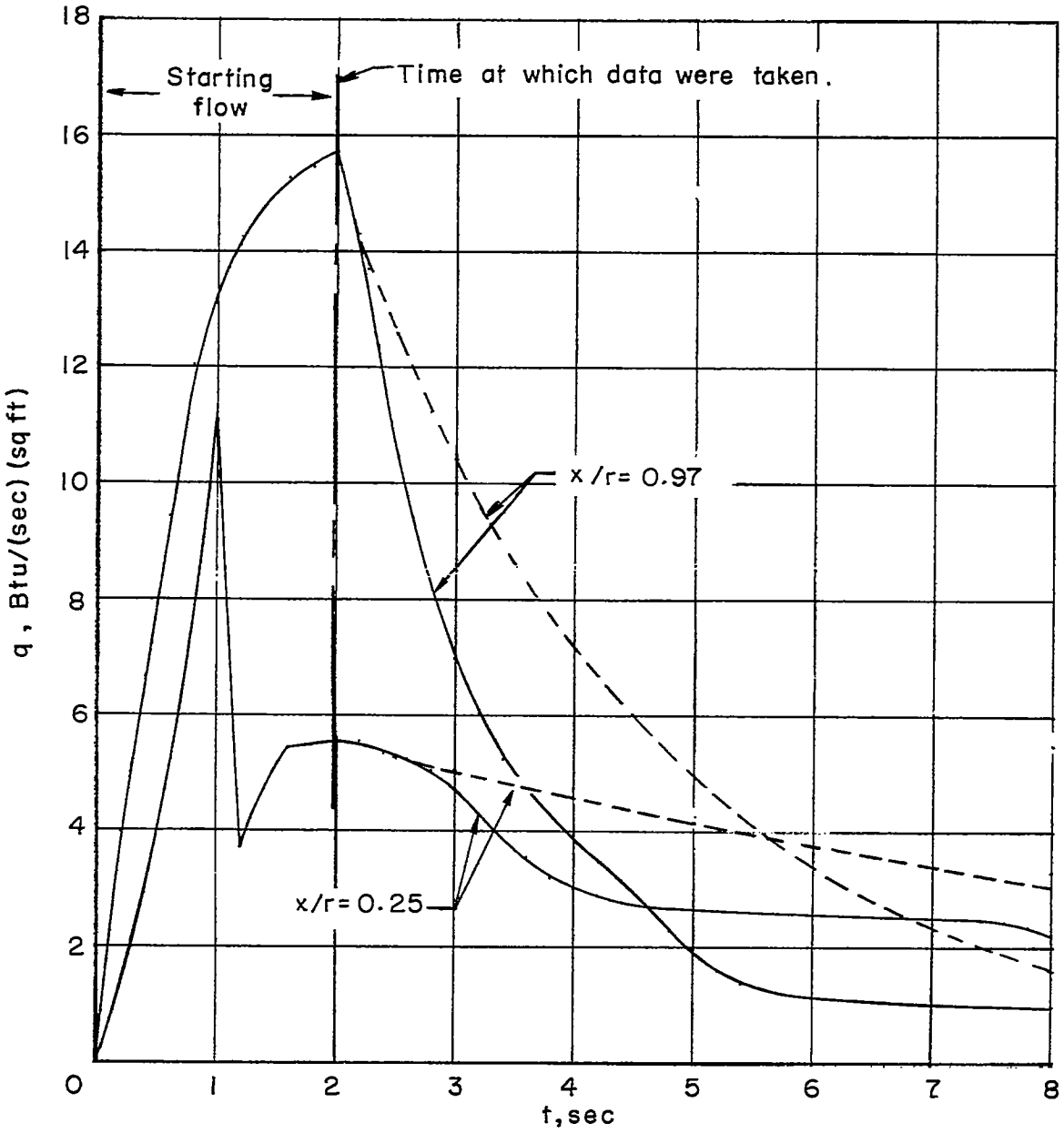

Figure 15.- Apparent heating rates from two typical temperature-time histories.

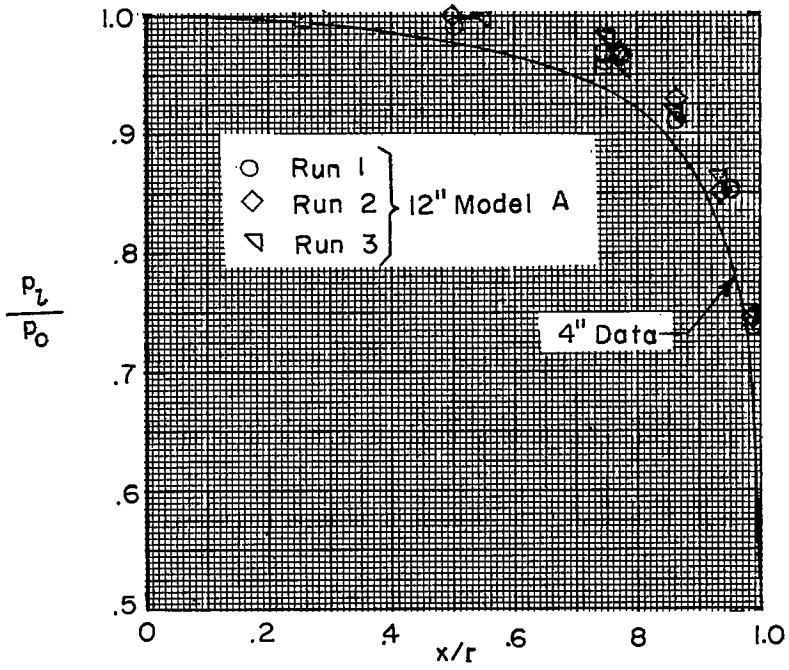

(a) Pressure measured along main ray of 12-inch model A.

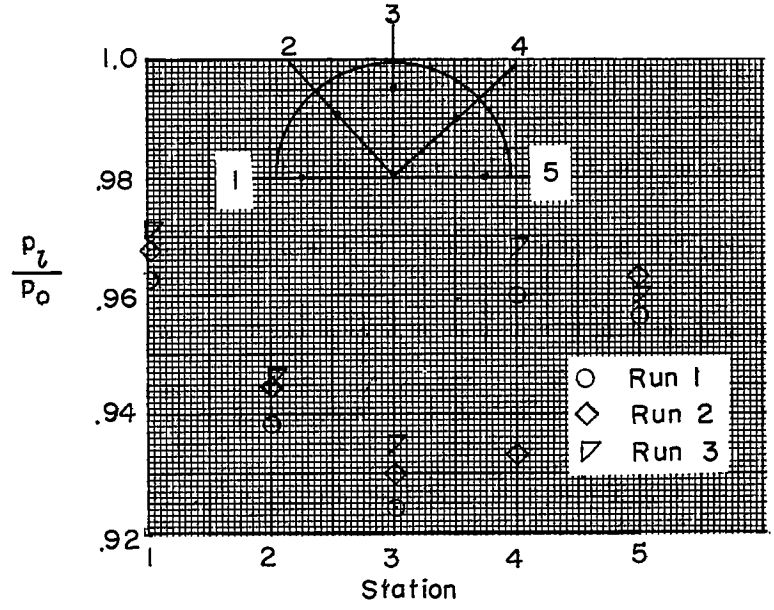

(b) Pressures at 75-percent station on model A.

Figure 16.- Pressure measured on 12-inch model.